The effect of temperature on the fracture mechanism in 2014Al/15vol.%Al_2O_3 composite

D.-G. C. Syu and A. K. Ghosh

Department of Materials Science and Engineering, The University of Michigan, Ann Arbor, MI 48109-2136 (USA)

(Received August 10, 1992; in revised form August 2, 1993)

Abstract

The tensile fracture strain, stress and fracture mode for a discontinuously reinforced aluminum matrix composite, 2014Al/15vol.%Al_2O_3, were determined and compared with those of the unreinforced matrix material, 2014Al, at various temperatures. Tests were conducted under uniaxial tension at elevated temperatures with a strain rate of 0.1 s^{-1}. It was found that the tensile fracture strain as well as fracture stress of the composite were lower than those of the matrix material. The tensile fracture mode changed from transgranular fracture to intergranular fracture between 400 °C and 500 °C for both materials. For the composite, at temperatures below 400 °C the growth and coalescence of voids occurred via a dislocation creep process primarily along the Al–Al_2O_3 interface. Above 400 °C voids initiated and grew at the Al–Al_2O_3 interface and grain boundaries via a diffusion creep process. The void growth was found not along the tensile direction but along the Al–Al_2O_3 interface and grain boundaries, and this resulted in a low fracture strain. A method for determining quantitatively the characteristics of the void initiation and growth is discussed.

1. Introduction

It has been reported experimentally and analytically by many researchers [1–4] that at ambient temperature inclusions in a ductile matrix exert considerable influence on the nucleation and propagation of cracks which lead to fracture. The fracture process usually follows three different stages for this type of ductile fracture: (1) formation of cracks at inclusions, (2) growth of cracks and (3) internal restriction leading to crack coalescence and failure. As the volume fraction of inclusions increases, fracture proceeds through a transition towards brittleness and shows increasing amounts of flat facets and cleavage fracture, especially in b.c.c. materials.

For discontinuously reinforced aluminum (DRA) matrix composites at ambient temperature, the fracture process is similar to the above three stages. However, the ductility is dependent not only on the reinforcement volume fraction but also on the matrix temper [5, 6]. McDanels [5], Christman [6] and Lewandowski *et al.* [7] showed that the primary mode of tensile fracture with an underaged matrix of Al/SiC metal-matrix composite was SiC particle fracture with preferential fracture at the larger particles. As overaging increased, the toughness of the composites was not recovered. This can be ascribed to precipitation at the Al–SiC interface which reduces the bond strength between Al and SiC, and results in an increasing proportion of fracture near the Al–SiC interface at the expense of particle fracture [7].

At elevated temperature, there are basically three kinds of ductile tensile fracture modes [8, 9]. They are rupture, transgranular creep fracture and intergranular creep fracture, as shown in Fig. 1.

For DRA matrix composites, most tensile fracture is due to the transgranular creep fracture at elevated temperature [10]. Nieh *et al.* [10] tested 6061Al/SiC particulate and 6061Al/SiC whisker composites and concluded that the fracture surfaces had similar features in both the particulate and whisker reinforced composites. Both exhibited the transgranular creep fracture and failed by plastic tearing of the Al matrix. They also found that there was essentially a one-to-one correspondence between the SiC dispersoids and dimples of the fracture surface, indicating SiC particulates strongly influenced the cavitation process during the high-temperature tension test.

The main purpose of this investigation was to determine the fracture behavior in DRA composites at elevated temperature. We found that the presence of reinforcing particles in 2014Al/15vol.%Al_2O_3 composite significantly decreased the forging limit as compared with matrix alloys [11]. To study the origin of this effect, it is necessary to examine the fracture behavior in both the matrix material and the composite.

In the near-net-shape forging, the failure is defined as the appearance of the incipient cracks. However, the

0921-5093/94/$7.00
SSDI 0921-5093(93)09409-C

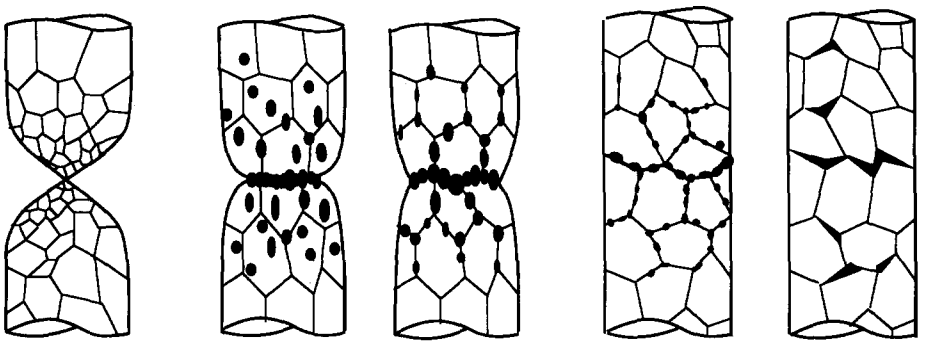

Fig. 1. Three typical modes of high-temperature tensile fracture: (a) rupture, (b) transgranular creep fracture and (c) intergranular creep fracture. Rupture is generally associated with dynamic recovery and/or recrystallization. Transgranular creep fracture requires either that holes pre-exist or that they nucleate at inclusions which concentrate stress. Intergranular creep fracture is characterized by grain-boundary sliding which causes void or crack nucleation by diffusional void growth along the grain boundary. (Courtesy of T. H. Courtney [8].)

incipient fracture is mainly caused by local stress or strain concentration at particle clusters by pre-existing porosites or by particle cracking etc. [12]. To study systematically the plastic deformation of fracture for a given material, it is necessary to record the stress–strain response until fracture ensues. Therefore, in the present work, tests were stopped when samples fractured rather than when incipient cracking occurred. According to the stress–strain response and examination of the microstructures, the deformation and fracture behaviors of material can be characterized.

2. Experimental procedures and results

2014 Al alloy and 2014 Al reinforced with 15 vol.% Al_2O_3 particles were used for the current study. The matrix alloy chemistry was Al–4%Cu–1%Mn–0.5%-Mg–0.8%Si–1.2%Ti. These materials were ingot cast and extruded (manufactured by Duralcan Aluminum Composites Corporation, San Diego, CA; the average particle size of Al_2O_3 was 5.6 μm). The average grain size in the matrix alloy was 500–2000 μm and the composite was 2–10 μm [11]. For fracture work, these materials were tested under uniaxial tension since, in a metal forming operation, fracture is usually caused by a tensile mode of deformation [11]. To characterize the failure behaviors of the materials, the fracture strain, fracture stress and fracture mode were determied from tensile tests of both the matrix material and the composite at various temperatures. Finally, an understanding of fracture mechanism for the composite at high temperatures is discussed using existing models.

2.1. Stress strain curve and temperature

To eliminate any contribution from anisotropy, both the matrix and composite materials were tested along the extrusion direction. The tensile specimens had a gage length of 11.11 mm [11]. For these tests, a medium strain rate of 0.1 s^{-1} was chosen to simulate conditions of forging at intermediate rates. The testing temperatures chosen were 300 °C, 400 °C and 500 °C with a heating rate of 30 °C min^{-1}. Samples were held at these temperatures for 10 min to stabilize the temperature, before testing on an Instron universal testing machine. Figure 2 shows the tensile σ–ε curves for 2014 Al and 2014Al/15vol.%Al_2O_3 at 300 °C, 400 °C and 500 °C. This figure shows that the flow stress of the composite is almost the same as that of the matrix material at 400 °C, but becomes less than that of the matrix material at 500 °C. If the yield stress (at 0.2% offset plastic strain) is plotted *vs.* temperature for each material, it is found that the two curves intersect at about 410 °C, as seen in Fig. 3 [11]. That is, below 410 °C, Al_2O_3 particles strengthen the matrix (for an applied strain rate of 0.1 s^{-1}), and above 410 °C a different deformation mechanism probably dominates which causes weakening of the composite. The same observation was also reported by Pickens *et al.* in 6061Al/20vol.%SiC and 7090Al/20vol.%SiC under a hot torsion test [13].

2.2. Fracture strain and temperature

The fracture strain was determined from the cross-sectional area at fracture for the tensile specimen. It is defined as $\ln(A_f/A_0)$, where A_0 is the starting cross-sectional area and A_f is the cross-sectional area of the fracture surface. The fracture area is determined from measurements of width and thickness of the fractured samples by a micrometer and an optical microscope, and averaged to minimize the errors. Figure 4(a) shows the fracture strains obtained at various temperatures; below 400 °C the fracture strains increase with increasing temperature, and above 400 °C this trend reverses

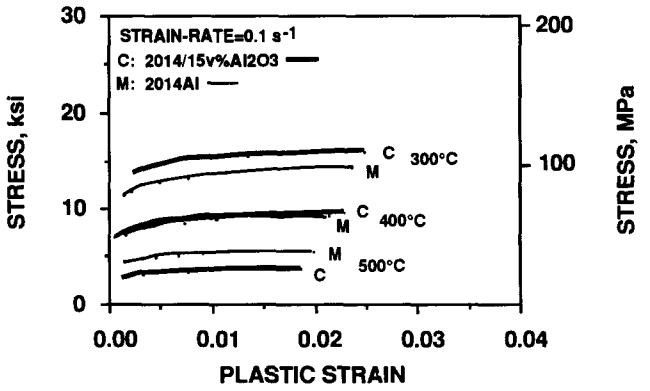

Fig. 2. Effect of particles on the σ–ε curves at various temperatures under uniaxial tension test along the extrusion direction. At 500 °C Al_2O_3 particles cannot strengthen the matrix.

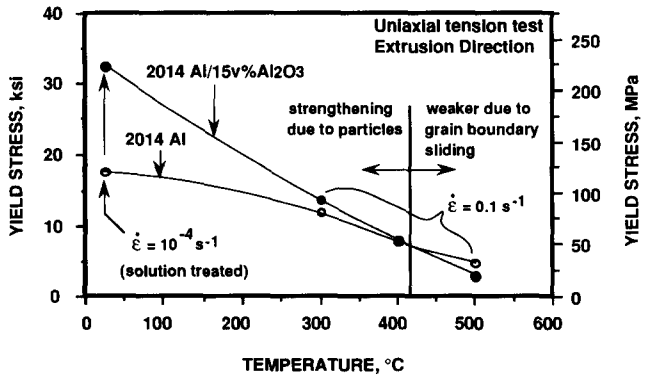

Fig. 3. Stresses selected from 0.2% plastic strain (yield stress) *vs.* temperature for 2014Al/15vol.%Al_2O_3 and 2014 Al. Above 410 °C the yield stress of 2014Al/15vol.%Al_2O_3 became lower than that of 2014 Al [11].

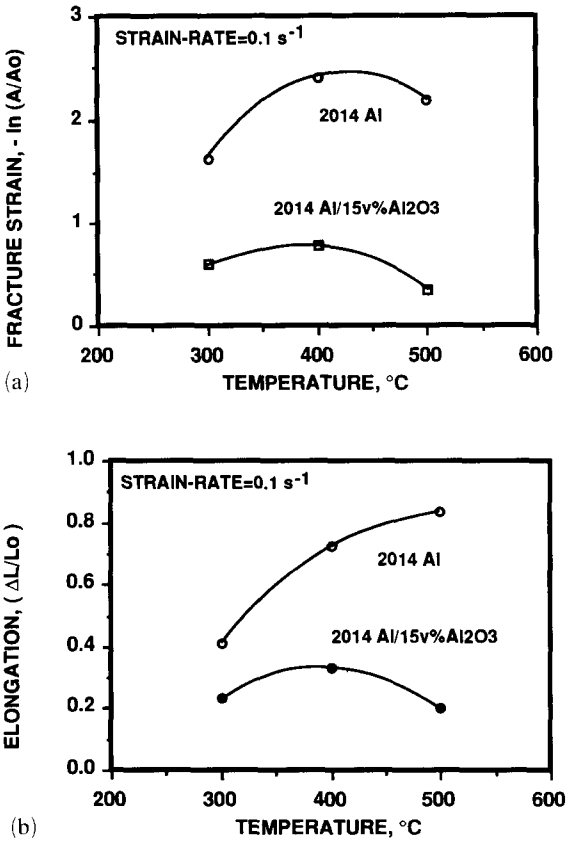

Fig. 4. (a) Fracture strain and (b) elongation *vs.* temperatures for 2014 Al and 2014Al/15vol.%Al_2O_3 under uniaxial tension test.

for both matrix and composite materials. This kind of ductility reversal trend was also reported by Pickens *et al.* in 6061Al/20vol.%SiC and 7090Al/20vol.%SiC under a hot torsion test [13] which has a different mode of instability. Figure 4(b) shows the elongations at various temperatures for 2014 Al and 2014Al/15vol.%Al_2O_3. In contrast to the fracture strain, the curve of elongation *vs.* temperature increases continuously with increasing temperature for the matrix material, but for the composite it reaches a maximum around 400 °C and then declines.

2.3. *Fracture stress and temperature*

The fracture stress was defined as the load at fracture divided by the cross-sectional area of the fracture surface A_f. To determine the fracture load, the following method was used. Because the response of the recorder pen after sample fracture is a linear drop of load with time, the point of departure from this linear segment provides a clear measure of fracture load, as shown in Fig. 5. The approach for the measurement of fracture area A_f has been discussed in Section 2.2. The relationships between fracture stress and temperature for 2014 Al and 2014Al/15vol.%Al_2O_3 are shown in Fig. 6, where the fracture stresses for both materials decrease with increasing temperature. It is also seen that the fracture stress of the composite is less than that of the matrix material at all temperatures.

2.4. *Fracture mode, fracture mechanism and temperature*

The tensile fracture surfaces were examined by using scanning electron microscopy (SEM) to study the fracture mode for both matrix and composite materials. For the composite, the tensile fracture mode at ambient temperature was a "dimpled" ductile fracture mode, as seen in Fig. 7. The dimple centers were the locations of the particles responsible for microcrack initiation. The material between the dimples is the matrix whose separation has been accomplished by void link-up during extensive plastic flow, as was reported in refs. 7 and 14.

The fracture surfaces of the matrix alloy at 300 °C, 400 °C and 500 °C are shown in Figs. 8(a), (b) and (c)

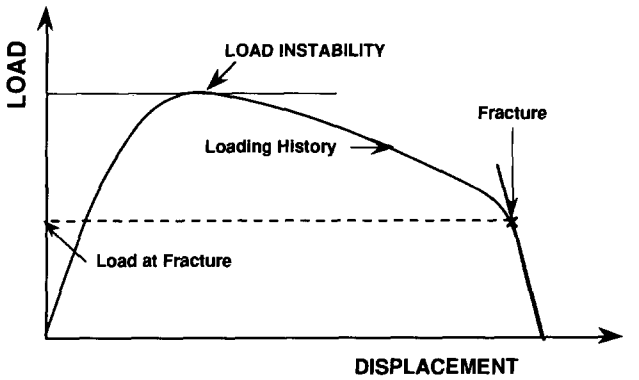

Fig. 5. Schematic diagram of a typical charge of load *vs.* displacement for high temperature uniaxial tension test.

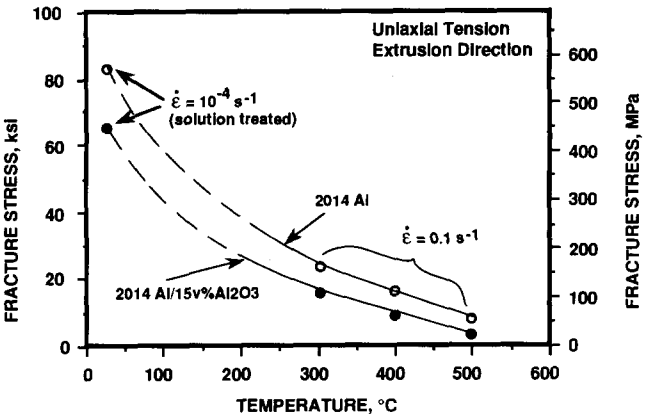

Fig. 6. The fracture stress decreased with increasing temperature for both 2014 Al and 2014Al/15vol.%Al_2O_3 under uniaxial tension. The fracture stresses of the matrix material at various temperatures are higher than those of the composite.

respectively. The fracture modes at 300 °C and 400 °C were found to be similar to that for transgranular creep fracture (ductile dimple type) and different from that at 500 °C, where failure occurred by intergranular creep fracture.

Figures 9(a), (b) and (c) show the fracture surfaces of the composite at 300 °C, 400 °C and 500 °C respectively. The fracture modes at 300 °C and 400 °C were the same, and both exhibited transgranular creep fracture. Some Al_2O_3 particles were also found in the dimple centers, while it appears that many particles were dislodged, possibly owing to relief of residual stresses at high temperatures. The fracture mode at 500 °C was by intergranular creep and revealed grain boundary cracking. It also appears that after 500 °C deformation the grain size was not significantly different from that of the starting material.

Deformed composite samples were polished to observe the microscopic damage mechanism. Figures 10(a), (b) and (c) show micrographs adjacent to the

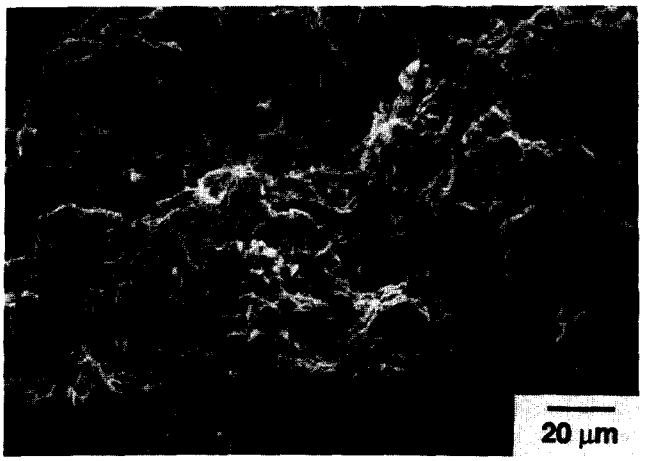

Fig. 7. SEM fractograph of 2014Al/15vol.%Al_2O_3 under uniaxial tension at room temperature and a strain rate of 10^{-4} s^{-1}. The matrix appears to have ductile fracture and Al_2O_3 particles are at the center of dimples.

fracture surface for the composite at 300 °C, 400 °C and 500 °C respectively. At 300 °C and 400 °C most voids initiated and grew at the Al–Al_2O_3 interface along the tensile direction, and their coalescence eventually caused the fracture. Some microcracks at grain boundaries were also seen in the matrix at 400 °C. However, at 500 °C only a few microvoids nucleated at the Al–Al_2O_3 interface. Before these voids could grow along the tensile direction, the cracks propagating normal to the tensile direction had progressed and caused fracture. This kind of intergranular creep fracture is discussed in more detail in the next section.

To understand quantitatively the change in fracture mechanism as a function of temperature, profiles of the fracture region were examined from mounted specimens. The void formation within the composite was quantified by measuring the void area from micrographs using the following method [15, 16]. A series of SEM images was taken from the sample profile at several selected regions. The plastic strains at these selected regions were determined by measuring the true strain in area reduction, as seen in Fig. 11(a). In a selected area of 300 μm × 120 μm, the fraction of void area was determined from the area occupied by voids divided by the total area (300 μm × 120 μm). Figure 12(a) shows the relationship between the plastic strain and the fraction of void area; voids do not initiate before a plastic strain of 0.6 at 400 °C, however, there is a rapid growth beyond this point. At 500 °C this incubation strain is about 0.3 and the sample fails with a much lower void volume fraction.

It has been found that at high temperatures fracture can occur in regions of specimens exhibiting somewhat lower void area fraction. This happens because voids and cracks do not always grow along the tensile

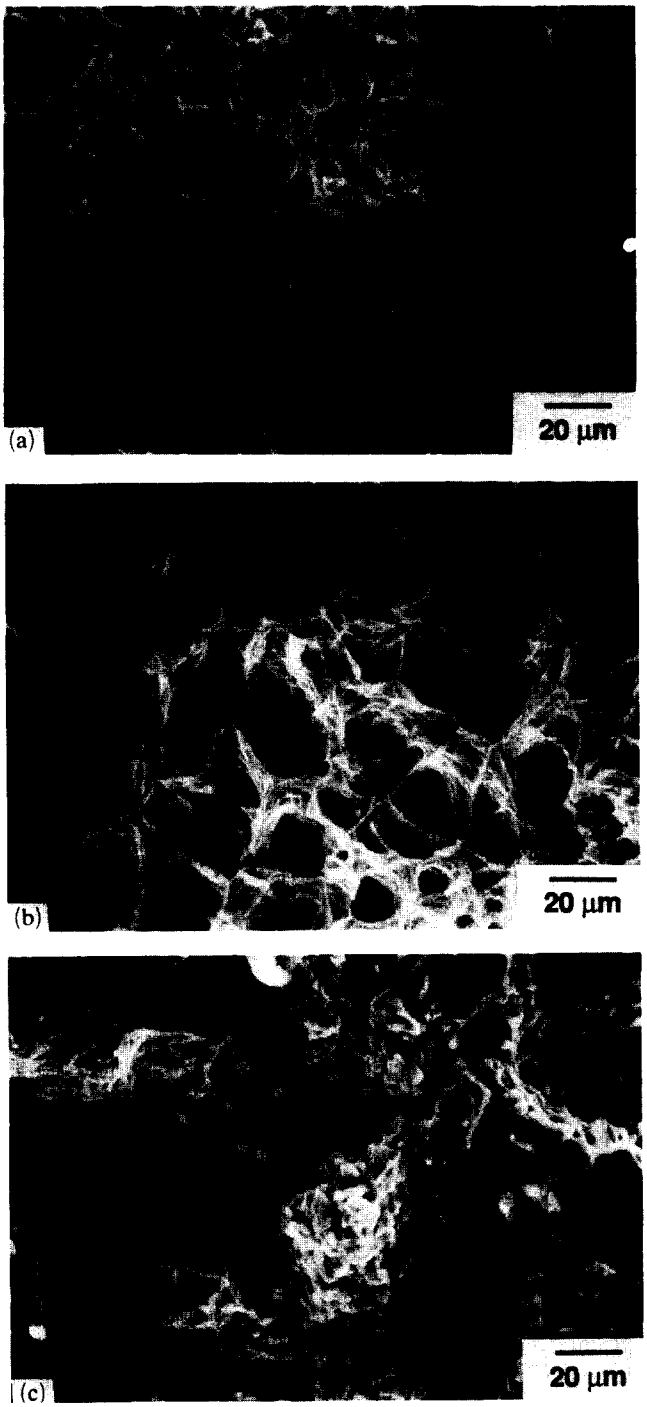

Fig. 8. SEM fractographs of 2014 Al under uniaxial tension test with a strain rate of 0.1 s^{-1} at (a) 300 °C, (b) 400 °C and (c) 500 °C. The fracture mode is intergranular at 500 °C, and ductile "dimple" type at 300 °C and 400 °C.

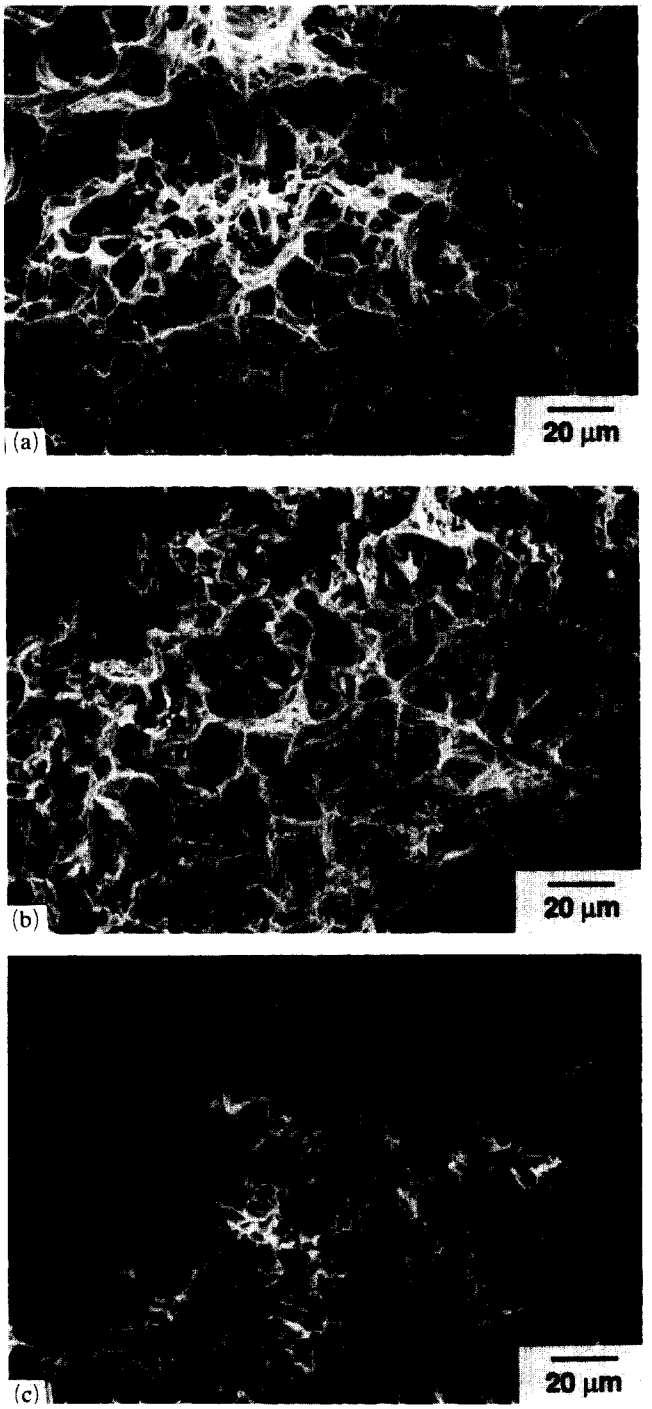

Fig. 9. SEM fractographs of 2014Al/15vol.%Al_2O_3 under uniaxial tension test with a strain rate of 0.1 s^{-1} at (a) 300 °C, (b) 400 °C and (c) 500 °C. The fracture mode is intergranular at 500 °C, and ductile "dimple" type at 300 °C and 400 °C.

direction but propagate nearly normal to the tensile direction at 500 °C. Thus, to assess the proximity to fracture at high temperatures, the total cavity volume may not always be the best indicator. Therefore, another approach was used to analyze the microscopic damage process. This method was as follows. An area of 200 $\mu m \times 20$ μm was chosen to measure the fraction of void projection length. The fraction of void projection length is defined as the total projection length of voids on the selected length divided by total length, as shown in Fig. 11(b). The reason for measuring the void projection length is to trace the void or crack propaga-

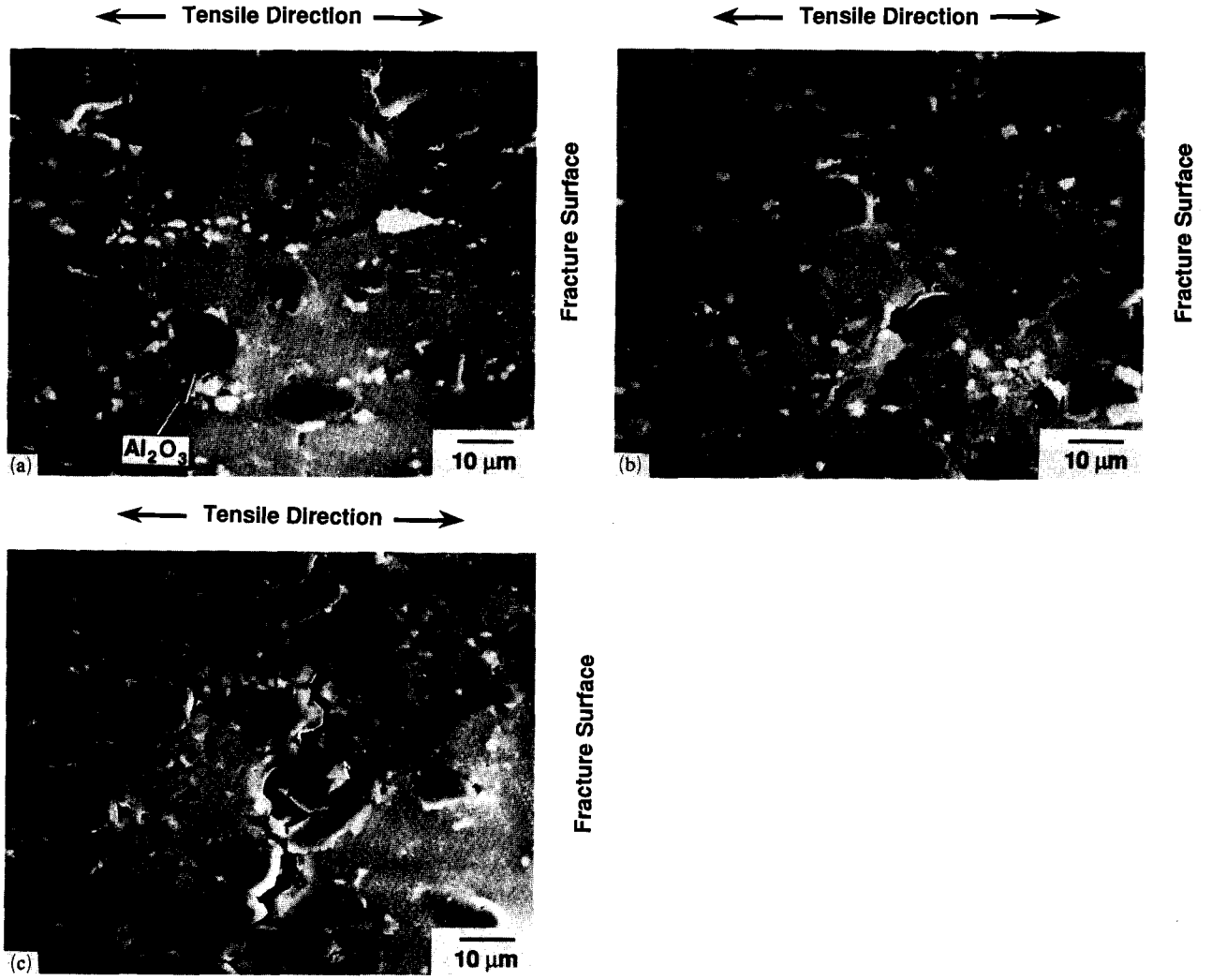

Fig. 10. SEM images near the fracture surface for 2014Al/15vol.%Al_2O_3 under uniaxial tension at (a) 300 °C, (b) 400 °C and (c) 500 °C with a strain rate of 0.1 s^{-1}.

tion path normal to the tensile direction. It is clear that once the void projection lengths entirely join each other, separation of the tensile specimen occurs. The fractions of void projection length at three adjacent regions were measured to obtain an average value at a given plastic strain. Figure 12(b) shows the average fraction of void projection length plotted as a function of plastic strain. We see that the projection length of voids at 500 °C increases more rapidly than that at 400 °C within a small plastic strain range. In addition, the projected void fraction is larger at 500 °C than at 400 °C, even though at a corresponding strain level the fraction of total void area at 400 °C is larger.

3. Discussion

We found that the as-extruded 2014 Al matrix material has a grain size of 500–2000 μm, while the composite in the same condition has a grain size of 2–10 μm [17]. We also noted that the high-temperature deformation of Al/Al_2O_3 composites is controlled by the matrix grain size [18, 19]. In Fig. 3 the Al_2O_3 particles appear to strengthen the 2014 matrix below 410 °C. However, the finer matrix grain size seems to weaken the composite material above 410 °C at a strain rate of 0.1 s^{-1}. This is believed to be a result of grain boundary diffusion creep which is dominant at such temperatures [20–22]. Thus, at elevated temperature, the weakening of the matrix within the composite relative to the unreinforced matrix alloy overcomes any strengthening effect associated with particles. For instance, an estimate of the diffusion creep rate in aluminum alloys using Coble's creep law shows that the finer grain matrix in the composite can deform at a rate 10^6–10^7 times faster than the unreinforced matrix alloy. This creep rate is so much faster than that of the coarse

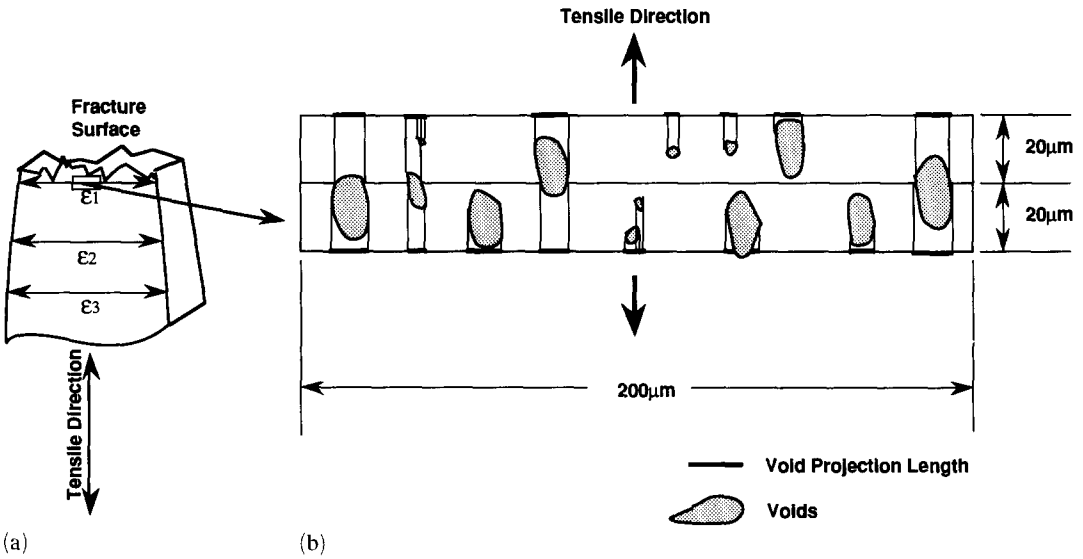

Fig. 11. Schematic diagrams illustrating (a) a section of a tensile specimen with different levels of strain near fracture and (b) determination of void projection lengths for a given plastic strain.

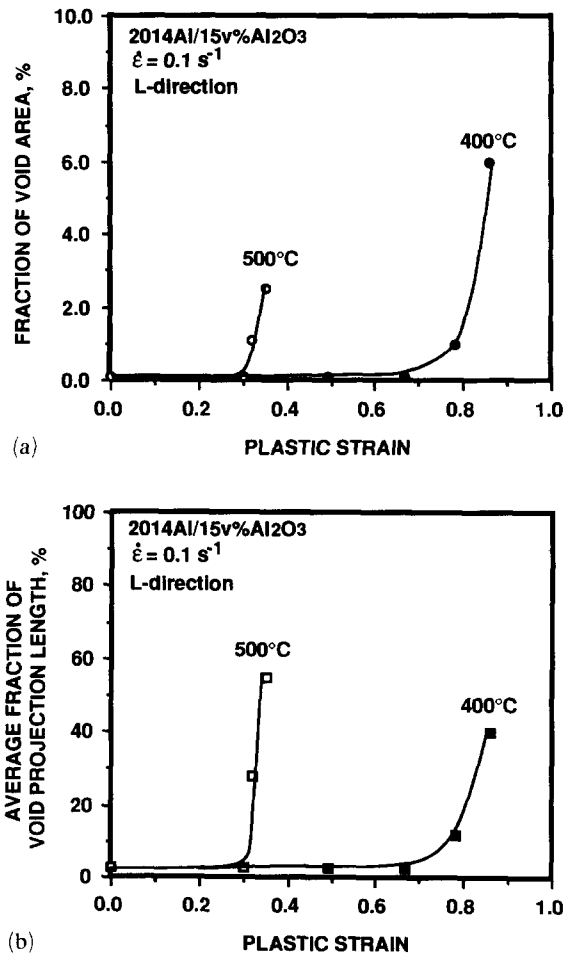

Fig. 12. (a) Fraction of void area and (b) average fraction of void projection length at 400 °C and 500 °C plotted as a function of plastic strain for 2014Al/15vol.%Al_2O_3 under uniaxial tension.

grain matrix that it can easily offset any reinforcement effect of Al_2O_3 particles.

For both materials the fracture modes changed from transgranular (ductile) to intergranular (less ductile) creep fracture between 400 °C and 500 °C. This is believed to be the reason why the fracture strain at 500 °C was lower than that at 400 °C for both materials.

For the composite, at 400 °C some grain boundary cracking was observed near the fracture surface, as seen in Fig. 10(b). However, its effect on fracture was less than that of the growth and coalescence of voids, as indicated by the appearance of the "dimples" at the fracture surface. Most voids at 300 °C and 400 °C were seen at the Al–Al_2O_3 interface and extended along the tensile direction, possibly owing to dislocation creep strain within the matrix [9]. Figure 10(c) shows that at 500 °C cracks and voids initiate at grain boundaries and Al–Al_2O_3 interfaces. However, the voids and cracks propagate along the grain boundaries and interfaces, rather than growing along the tensile direction as seen at lower temperatures.

To explain the present observation, a high-temperature fracture model is adopted from the work of Ashby *et al.* [9]. This is slightly modified for DRA composites and is illustrated in Figs. 13(a) and (b). At lower temperatures (*i.e.* 300 °C and 400 °C), the Al–Al_2O_3 interface is the preferential site (rather than grain boundaries) for void nucleation within the matrix. This may be exacerated further by precipitate particles in that region. The subsequent void growth along the tensile direction and coalescence of voids via dislocation creep of the matrix ligaments eventually cause

fracture, as shown in Fig. 13(a). This kind of fracture behavior has also been reported for materials containing small inclusions [1–4, 15] and for Al/SiC composites [7, 10, 23].

At higher temperatures (*i.e.* 500 °C) cracks and voids still initiate at grain boundaries as well as at $Al–Al_2O_3$ interfaces. However, grain boundary diffusion at voids and cracking along the grain boundaries and at $Al–Al_2O_3$ interfaces dominate the fracture process. The surface diffusion at voids maintains the void shape during boundary diffusional processes, *i.e.* the void growth is not along the tensile direction but along the grain boundaries and the interfaces, as shown in Fig. 13(b). Therefore, the resistance to crack propagation along the grain boundaries and $Al–Al_2O_3$ interfaces decreases as the temperature increases to 500 °C [9, 24–27]. It appears that at 500 °C, the rate of diffusional void growth along grain boundaries and interfaces becomes higher than that of void growth and coalescence along the tensile direction as seen at lower temperatures. This is also supported by the rapid increase in the void projection length near fracture at 500 °C over that at 400 °C as seen in Fig. 12(b). In addition, the projected void fraction is larger at 500 °C than at 400 °C, even though at the same strain the overall fraction of void area at 400 °C is larger.

The effect of oxygen induced corrosion in grain boundary cracking is not believed to be important here because aluminum-based alloys have a protective oxide coating on the surface which prevents further ingress of oxygen [28]. In addition, the high deformation rate and the internal cracks observed negate any possibility of oxygen induced corrosion. This aluminum oxide layer at the sample surface can also prevent the corrosion at grain boundaries or $Al–Al_2O_3$ interfaces within the material. Thus, the corrosion effect for the aluminum alloy can be ignored in the present case.

It has been seen during forging studies on this composite that the resistance to crack propagation and the fracture strain at 400 °C were greater than that at 300 °C owing to greater ductility at higher temperatures [12]. At both temperatures the growth and coalescence of voids were dominated by dislocation creep. However, as the temperature increased above 400 °C, the diffusional growth and coalescence of voids dominated, and the fracture strain decreased again. Thus, from the standpoint of forging or metal forming, the optimum temperature for this composite might be around 400 °C.

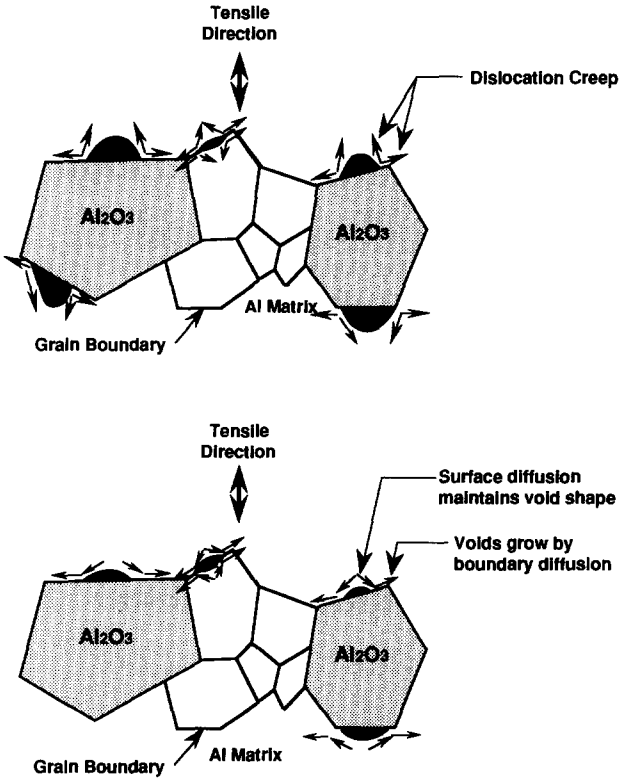

Fig. 13. Schematic diagrams illustrating void growth controlled by (a) a dislocation creep process and (b) a diffusion creep process in $Al–Al_2O_3$ metal matrix composites. The small arrows indicate the direction of material flow.

4. Conclusions

(1) The tensile fracture mechanism of 2014Al/15vol.%Al_2O_3 at 300 °C and 400 °C was mainly void nucleation at the Al_2O_3 interfaces, growth along the tensile direction, and coalescence of the growing voids. Dislocation creep was the main deformation process responsible for plastic flow at these temperatures. Above 400 °C, the voids or cracks nucleated at grain boundaries and $Al–Al_2O_3$ interfaces owing to grain boundary sliding and diffusion. Surface diffusion at voids maintained the void shape which minimized void growth along the tensile direction and caused cracks to propagate mostly along grain boundaries and $Al–Al_2O_3$ interfaces.

(2) The tensile fracture strains and stresses of 2014 Al at various temperatures were higher than those of the composite. Above 410 °C, the flow stress of the composite was less than that of 2014 Al. This weakening is believed to be due to increasing creep rate with decreasing grain size (in the composite matrix).

(3) The resistance to crack propagation during forging and the fracture strain at 400 °C were greater than that at 300 °C. As the temperature increased above 400 °C, the diffusion creep process gradually dominated the growth and coalescence of voids, and lowered the fracture strain. Thus, the optimum forging temperature for 2014Al/15vol.%Al_2O_3 is approximately 400 °C.

Acknowledgment

The authors would like to thank the AES, GM Technical Center for supporting this work. Fruitful discussions with Dr. B. Taylor of GM-AES are gratefully acknowledged.

References

1 J. Gurland and J. Plateau, The mechanism of ductile rupture of metals containing inclusions, *Trans. ASM, 56* (1963) 442–454.
2 J. R. Fisher and J. Gurland, Void nucleation in spheroidized carbon steels, part I: experimental, *Met. Sci., 15* (May 1981) 185–192.
3 J. R. Fisher and J. Gurland, Void nucleation in spheroidized carbon steels, part II: model, *Met. Sci., 15* (May 1981) 193–202.
4 J. N. Goodier, Concentration of stress around spherical and cylindrical inclusions and flaws, *ASME J. Appl. Mech., 55* (1933) 39–44.
5 D. L. McDanels, Analysis of stress–strain, fracture and ductility behavior of aluminum matrix composites containing discontinuous silicon carbide reinforcement, *NASA Rep. NASA TM-83610*, NASA Lewis, Cleveland, OH, 1984.
6 T. Christman, A. Needleman, S. Nutt and S. Suresh, On microstructural evolution and micromechanical modelling of deformation of whisker-reinforced metal-matrix composites, *Mater. Sci. Eng., A107* (1989) 49–61.
7 J. J. Lewandowski, C. Liu and W. H. Hunt, Jr., Microstructural effects on the fracture micromechanisms in 7XXX Al P/M-SiC particulate metal matrix composites, *Mater. Sci. Eng., A107* (1989) 241–255.
8 T. H. Courtney, *Mechanical Behavior of Materials*, McGraw-Hill, New York, 1990, pp. 503–508.
9 M. F. Ashby, C. Gandhi and D. M. R. Taplin, Overview No. 3, fracture-mechanism maps and their construction for F.C.C. metals and alloys, *Acta Metall., 27* (1979) 699–729.
10 T. G. Nieh, K. Xia and T. G. Langdon, Mechanical properties of discontinuous SiC reinforced aluminum composites at elevated temperatures, *ASME J. Eng. Mater. Technol., 110* (1988) 77–82.
11 D.-G. C. Syu and A. K. Ghosh, Forging limits for an aluminum matrix composite, Part I, Analysis, accepted for publication in *Metall. Trans. A*, 1994.
12 D.-G. C. Syu and A. K. Ghosh, Forging limits for an aluminum matrix composite, Part II, Experimental results, accepted for publication in *Metall. Trans. A*, 1994.
13 J. R. Pickens, T. J. Langan, R. O. England and M. Liebson, A study of the hot-working behavior of SiC–Al alloy composites and their matrix alloys by hot torsion testing, *Metall. Trans. A, 18* (1987) 303–312.
14 B. D. Flinn, M. Ruhle and A. G. Evans, Toughening on composites of Al_2O_3 reinforced with Al, *Acta Metall., 37* (11) (1989) 3001–3006.
15 B. A. Senior, F. W. Noble and B. L. Eyre, The nucleation and growth of voids at carbides in 9Cr–1Mo steel, *Acta Metall., 34* (7) (1986) 1321–1327.
16 M. W. Mahoney and A. K. Ghosh, Superplasticity in a high strength powder aluminium alloy with and without SiC reinforcement, *Metall. Trans. A, 18* (1987) 653–661.
17 D.-G. C. Syu and A. K. Ghosh, Stress-state dependence of strain hardening behavior in 2014 Al/15v%Al_2O_3 composite, accepted for publication in *Metall. Trans. A*, 1994.
18 A. E. Geckinli, Grain boundary sliding model for superplastic deformation, *Met. Sci., 17* (1983) 12–18.
19 A. K. Ghosh and R. Raj, A deformation model for elevated temperature including grain size distribution effects, *Mechanical Testing for Deformation Model Development, ASTM STP 765*, ASTM, Philadelphia, PA, 1982, pp. 415–434.
20 T. G. Langdon and R. B. Vastava, An evaluation of deformation models for grain boundary sliding, *Mechanical Testing for Deformation Model Development, ASTM STP 765*, ASTM, Philadelphia, PA, 1982, pp. 435–451.
21 R. Becker, A. Needleman, S. Suresh, V. Tvergaard and A. K. Vasudevan, An analysis of ductile failure by grain boundary void growth, *Acta Metall., 37* (1) (1989) 99–120.
22 A. Needleman, A continuum model for void nucleation by inclusion debonding, *ASME J. Appl. Mech., 54* (1987) 525–531.
23 F. J. Humphreys, W. S. Miller and M. R. Djazeb, Microstructural development during thermomechanical processing of particulate metal-matrix composites, *Mater. Sci. Technol., 6* (1990) 1157–1166.
24 J. C. Earthman and W. D. Nix, Simulations of stable crack propagation based on cavity growth by coupled diffusional and creep processes, *Acta Metall., 35* (7) (1987) 1475–1485.
25 S. J. Fariborz, D. G. Harlow and T. J. Delph, Intergranular creep cavitation with time-discrete stochastic nucleation, *Acta Metall., 34* (7) (1986) 1433–1441.
26 J. S. Wang and W. D. Nix, High temperature creep and fracture properties of a class I solid solution alloy: Cu–2.5 at.% Sn, *Acta Metall., 34* (3) (1986) 545–555.
27 D. S. Wilkinson, The effect of time dependent void density on grain boundary creep fracture—I continuous void coalescence, *Acta Metall., 35* (6) (1987) 1251–1259.
28 D. R. Gaskell, *Introduction to Metallurgical Thermodynamics*, McGraw-Hill, New York, 1981, 2nd edn.